LA-UR- 00-2259

POWDER DENSIFICATION MODEL OPTIMIZATION AND EXPERIMENTATION USING GENETIC ALGOTRITHMS

Brian J. Reardon

Materials Science and Technology Division
Los Alamos National Laboratory
Los Alamos, New Mexico 87545

ABSTRACT

Developing accurate, physics based, micromechanical, powder consolidation and sintering models with a minimum of experimentation constitutes an inverse and ill-posed problem that is most tractable through the application of Bayesian inference and genetic algorithms (GA). In this work, 19 consolidation model parameters are determined for two different Molybdenum (Mo) powders. The two powders differ in particle size distribution and morphology. Given limited and uncertain experimental densification data sets for these two powders, the Bayesian enhanced GA optimizes the model parameters to specific ranges. The evolved distribution of the model parameters is then used to predict relative densities for consolidation and sintering conditions in which no experimental data yet exists. More experiments are necessary in the regimes of the resulting response surface with unacceptably high uncertainty. Thus, this procedure allows models to co-evolve with experiments such that more accurate models can be developed with a minimum of experimentation.

Additionally, this work will compare and contrast the implications of conducting principal component (PC) analysis on the *a posteriori* model covariance matrix versus the correlation matrix. Proper interpretation of the PCs reveals information on parameter correlations as well as sensitivities, provided the specific conditions in the optimization are met. These conditions will be discussed. Finally, the influence of the different powder formation methodologies on the optimal consolidation parameters will also be discussed.

INTRODUCTION

INTRODUCTION: MOLYBDENUM POWDER PROCESSING

Molybdenum (Mo) has many applications in the field of ballistics, due to its high density (10.22 g/cc), high melting point (2622C), high yield stress (758 MPa), and hardness at high temperatures. Mo also has excellent thermal and electrical conductivity and good erosion resistance [1]. Unfortunately, these qualities also contribute to Mo's disadvantages, namely, high cost and processing difficulties.

DISCLAIMER

DISCLAIMER

Portions of this document may be illegible in electronic image products. Images are produced from the best available original document.

Isotropic component properties are advantageous for some ballistic applications Thus, given the high strength and refractory nature of Mo, powder metallurgy is the preferred processing approach for producing Mo components with the desired isotropic qualities[2-4].

Ideally, proper process design allows for the production of parts with a specific relative density and degree of grain growth and a minimum of processing time, temperature, pressure, and material waste. However, the development of accurate models that provide a sufficient level of predictability can require expensive and time-consuming experimentation, which also is a factor in the overall waste stream and cost of production. Consequently, there exists a need to quickly evolve accurate physics based computer models with a minimum of experimentation. This goal has been shown to be achievable when model development and experimental design are allowed to co-evolve. One approach to this co-evolution is through the use of genetic algorithms and Bayesian inference.

INTRODUCTION: MICROMECHANICAL MODELING

Several types of computer models are commonly used to simulate powder consolidation. Ashby's micromechanical model assumes a dense random packing of monosized spheres that consolidate according to the mechanisms of yielding, diffusion, creep, and grain growth when heated and pressed.

Such a model can be used to create densification and grain growth maps for HIPing [5]. There are, however, limitations to micromechanical modeling. Namely, the model requires the optimization of 19 parameters, using experimental data sets that have a significant amount of uncertainty. This optimization is further complicated by the fact that such a physics based model does not easily subscribe to standard gradient based optimization techniques. Another constraint on the optimization technique used is that it must provide a reasonable sensitivity analysis and measure of correlation. Additionally, the values published for variables in densification work often vary from the actual values for a researcher's particular powder. This is caused by differences in powder morphology, particle size distributions, and forming methods. A procedure is needed that allows each researcher to optimize the model parameters with experimental data for his specific powder.

It should also be noted that most adjustments of model parameters are executed with only densification data. Thus grain growth or primary densification mechanism data are often ignored in the model development. In the long term, this practice presents a problem since different parameters might fit the densification data equally well but result in different dominant densification mechanisms and grain growth maps.

Fitting the model to experimental data is an inverse and ill-posed problem requiring advanced optimization techniques. This study used Bayesian enhanced genetic algorithms to optimize the parameters of the micromechanical model. A brief description of Bayesian analysis and genetic algorithms follows, an extensive explanation was presented elsewhere [6-8].

INTRODUCTION: BAYESIAN ANALYSIS

The parameters that require optimization form a model parameter vector:

$$M=\{m_1, m_2,\ldots m_{19}\}^T \quad \text{Eq. 1}$$

The data vector is defined as:

$$D=\{d_1, d_2,\ldots d_N\}^T \quad \text{Eq. 2}$$

where N is the number of experimental data points.

The goal of Bayesian analysis is to accept or reject a particular model (M) given an experimental data set (D) and prior knowledge about the problem using Bayes' Theorem:

$$\sigma(M|D) = \frac{P(M,D)}{P(D)} = \frac{P(D|M)P(M)}{\int P(D,M)dM}. \quad \text{Eq.3}$$

$\sigma(M|D)$ is the posterior probability density (PPD). The theorem states that the conditional probability of a particular model M being correct given the data D is the ratio of the probability density function (PDF) of M and D to that of D alone. Although the individual components that make up the term P (D | M) are probabilities, the term itself is not a PDF but a likelihood function, and thus does not integrate to 1.0.

Unlike classical frequentist statistics, Bayesian analysis incorporates the researcher's subjective knowledge about the problem into the analysis, as shown by the dependence of the PPD on the prior PDF, P(M). Also, the PPD is updated as new experimental data becomes available, while frequentists would consider P(D) to be an unchanging distribution. Finally, a true frequentist considers it inappropriate to assign a probability of correctness to a hypothesis.

Bayes' theorem is a mathematical formulation of the scientific method. The theorem was first proposed by Rev. Bayes in 1763[9], but has not been used until recently due to computational difficulties in solving the probability integral:

$$P(D) = \int P(D,M)dM, \quad \text{Eq.4}$$

where the integral is formally carried over the entire N-dimensional model parameter space. An excellent introduction to Bayesian statistics is given in chapter 4 of Antelman [10].

The fast and accurate approximation of an N-dimensional, discontinuous PDF is the topic of many papers. Techniques for finding the PPD include Monte Carlo integration, Gibb's sampling, and genetic algorithms [11-15].

With an optimized PPD in hand, a number of characteristic metrics are easily obtained. For example, the expectation model is derived from the PPD by:

$$\langle M \rangle = \int M\sigma(M|D)dM. \quad \text{Eq. 5}$$

The PPD is normalized prior to finding the expectation.

The *a posteriori* model covariance matrix C_M is given by:

$$C_M = \int (M - \langle M \rangle)(M - \langle M \rangle)^T \sigma(M|D)dM. \quad \text{Eq. 6}$$

The standard deviation associated with the mean model is obtained through the square roots of the diagonal elements of C_M. Normalization of C_M through:

$$C_{ij}^* = \frac{C_{ij}}{\sqrt{C_{ii}}\sqrt{C_{jj}}}, \quad \text{Eq. 7}$$

produces the correlation matrix.

With C_M and C_M^* determined, principal component analysis (PCA) provides valuable insight on the degree of variance and correlation among the variables. In PCA, the C_M or C_M^* is transformed into a new set of axes that are orthogonal to each other and are ordered based on the variance associated with that axis. The principle components are obtained by computing the set of eigenvalues (λ) and corresponding orthogonal eigenvectors (U)such that:

$$C_M = U \lambda U^T \quad \text{Eq. 8}$$

is satisfied. In a d-dimensional variable space, there are d eigenvalues or principle components. However, many principle components, derived from the correlation matrix, may have variances less than one and thus the intrinsic dimensionality is k where $k < d$. The cut off eigenvalue of 1.0 is not rigorously defined for all situations and thus some authors recommend a cut off of 0.7. In the case of the covariance matrix, a cutoff of value of $0.7\bar{\lambda}$ is recommended where $\bar{\lambda}$ is the average eigenvalue[16].

As implied above, PCA of C_M^* does not necessarily generate the same eigenvalue distribution as that of C_M. This is especially true if the variables that constitute C_M differ dramatically in value. In such a situation, the principal components are usually dominated by the largest valued variables. For this reason it is recommend that PCA be conducted on the correlation matrix.

Different forms of Bayesian analysis have been used in the materials science arena to assist in fitting models to data such that the model obtains a quantifiable predictive capacity. In this work, the Bayesian analysis is used to better understand the output of a genetic algorithm (GA). The GA is used to optimize the parameters of a discontinuous physics based micromechanical powder densification model.

INTRODUCTION: GENETIC ALGORITHMS

Evolution is an intrinsically robust search and optimization procedure. Evolved organisms have optimized solutions to complex problems at every level of organization, from organelles to ecosystems. The problems that biota have solved and continue to improve upon, are typified by chaos, chance, temporality, nonlinearly, and multidimensionality. Such problems are intractable to deterministic optimization techniques, especially in situations where heuristic solutions are not available.

GA's are a type of evolutionary algorithm, algorithms that attempt to mimic the processes of evolution in optimization. The essence of such a simulation lies in expressing the solution to a problem not as a single value, but as a string of fundamental building blocks (genes). These building blocks can be manipulated in much the same way as an extant species manipulates its gene pool, through selection and mating to produce offspring more suited to the current environment. For example, consider x_1, which is a member of a population of feasible solutions to a problem, but not necessarily the optimal solution. The real value of x_1 is expressed as a string of binary digits, e.g.: 011001110, that is L digits long. This binary string is mapped to a real value of x_1 such that the string 1111111 corresponds to the maximum value of x in the search range, and 0000000 corresponds to the minimum x value. If a function requires the optimization of more than one variable, f(x,y), then the total string for a specific member is formed by placing the binary digits defining x and y back to back in one string. For example if $x_1 = 001100$ and $y_1 = 110001$, then the string for member 1 would be 001100110001.

Manipulation of these strings occurs in much the same way chromosomes are manipulated in evolving species. First, competition among members of the population determines who is most fit or optimal. Second, the most optimal members are allowed to reproduce. Reproduction involves slicing the chromosomes of the two members of the populations and then exchanging segments:

$$\begin{matrix} X_1 : 10100011 \\ X_2 : \underline{11110111} \end{matrix} \rightarrow \begin{matrix} \tilde{x}_1 : 1010\underline{0111} \\ \tilde{x}_2 : \underline{1111}0011 \end{matrix} \qquad \text{Eq. 9}$$

where $\tilde{X}_1$ and $\tilde{X}_2$, the resulting progeny, are placed in the next generation. The actual crossover site is randomly selected with some probability, p_c. Third, mutation occurs which in a positively entropic system ensures genetic diversity in the subsequent generation. Mutation involves flipping the value of a randomly selected bit, which is defined by some probability p_m. The new population that evolves from the selection, crossover, and mutation operators is defined as a generation. This cycle is repeated for a number of generations as specified by the user [17]. The strength and novelty of the GA lays in how selection of members is conducted when dealing with multiple, conflicting, poorly defined objectives. The selection procedure uses a fuzzy logic normalization scheme as well as continuously updated phenotypic niching. A more detailed discussion of the selection procedure is found elsewhere [6].

The GA acts as a Bayesian Inference Engine (BIE) in that it uses Bayes' Theorem to select members in the population for crossover, and thus the output of the GA is the PPD of Bayesian inference. The production of a PPD allows for many of the statistical tools available in Bayesian statistics to be applied to analyzing GA output. C_M, C_M^*, and <M> are derived from the PPD. Following the method outlined by Sen and Stoffa [11-12], a 2-D array of M by B is reserved where M is the number of parameters and B is

the number of values each variable can take (i.e. the number of bins). At each generation, an unnormalized PPD is calculated for each model and stored in the proper position in the bin array for each model parameter. At the end of the GA run, the model parameter PPD values are normalized. Each component of the vector for a particular parameter is stored and summed with corresponding values from other models, which provides <M>. C_M is determined by summing up $MM^T\sigma(M)$ in a square array of MM for each model and at the end of the run subtracting $<M><M>^T$.

Once the PPD, <M>, and C_M are sufficiently determined, the GA is stopped and optimal model parameter vectors are selected and used in the physics of the forward problem for conditions that have not been experimentally tested.

In the context of a PPD evolved by a GA, PCA is a powerful tool that assists in overcoming many deficiencies in GA's. First, as the population evolves, the sum of the eigenvalues of C_M approaches a limit. When the rate of change in the sum reaches an acceptable minimum, the GA can be stopped. Second, the largest eigenvalues and their corresponding eigenvectors indicate the variables or groups of variables with the greatest variance in the evolved population of models given the available data. Thus, PCA acts as a sensitivity analysis for the variables in the model. Once the PPD is determined to be reliable based on the stabilization of the eigenvalues, an optimum model is selected.

In this work, a GA is used to optimize the 19 parameters of a micromechanical powder densification model given limited and uncertain densification data sets. With the parameters optimized, a formal principle component analysis of the parameters is possible as well as the generation of densification and uncertainty maps that act as an experimental design guide.

PROCEDURE

Two Molybdenum powders were used in this study. They were formed using different methods and consequently have distinct physical characteristics. The properties of the powders can be found in Table I. Mo 21373SC (SC in Table I) was reduced from ammonium molybdate ($(NH_4)_2MoO_4$), and has a fine particle size. Conversely, the Mo 528SOMP (SOMP in Table I) was spray dried with a binder and reduced. This processing route resulted in the agglomeration of fine particles into a spherical morphology thus giving a large apparent particle size as indicated in Figure 1 and Table I. According to Table I, both powders have relatively low tap densities which will contribute to difficulties in fitting Ashby's micromechanical model to the densification data.

Table I. Properties of Mo SC and Mo SOMP powders

	SC	**SOMP**
Forming Process	Reduced from $(NH_4)_2MoO_4$	Spray dried with a binder and reduced
Pycnometer density (g/cc)	10.46	10.11
Apparent Density (%ρ_{th})	18.4	22.3
Tap Density (%ρ_{th})	33.6	27.8
Fisher Number	7.8	4.5
Median Particle Size (μm)	11.49	18.43
Particle Size Distribution	1-100	10-120
Surface Area (m^2/g)	0.266	0.492
C (ppm)	7.54	7.77
O (ppm)	1794	3937
N (ppm)	94.3	53

SC 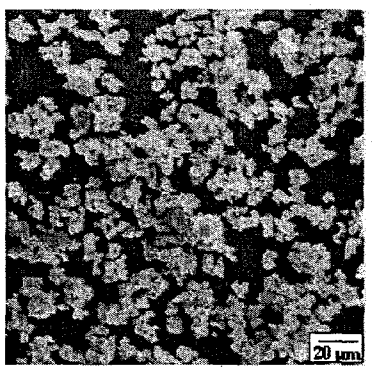 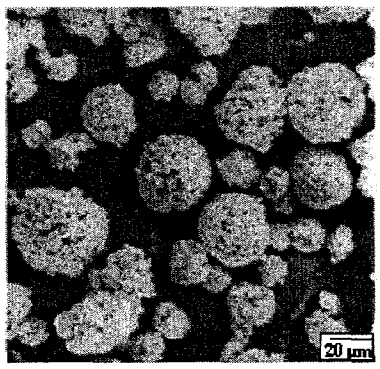 SOMP

Figure 1. SEM of Mo SC and Mo SOMP. While the SOMP particulates are 4-5 times larger than the SC particulates, one should keep in mind that the SOMP particulates are actually agglomerates of particles that are smaller than the SC particulates.

The first step in GA optimization was to determine the parameter ranges to be searched. The values used in this study, as indicated in Table II, came from literature and the guidelines of Ashby's work[5]. The search range is used to define the limits of the randomly selected initial population. This initial population (Generation 0) is then inserted into the physics of the forward problem to provide densification maps such as that shown in figure 2. In figure 2, the densities calculated for each temperature and pressure are determined by assuming a 1 hour ramp up to the specified temperatures and pressures, 1 hour hold, and 1 hour ramp down. Since a population of individuals was used in determining the average densification map, there is also a corresponding error map associated with the average. The maximum point in the error map indicates the area where more experimental data would be most helpful.

Table II. The *a priori* search ranges for each parameter in the micromechanical sintering model.

			Mo SOMP		**Mo SC**	
#	Parameter	Units	Lower bound	Upper bound	Lower bound	Upper bound
1	Surface Energy	J/m^2	1.00	3.00	1.00	5.00
2	Yield Stress	MPa	300.0	1000.0	200.0	700.0
3	Temperature Dependence of Yield		0.40	0.60	0.10	0.60
4	PLC Component		2.00	6.00	2.00	6.00
5	PLC Reference Stress	MPa	50.00	150.00	100.00	200.00
6	PLC Activation Energy	kJ/mol	300.00	500.00	350.00	450.00
7	Low T. to High T. Creep Transition	K	1400.0	1500.0	1400.0	1500.0
8	C for Low T. Creep		0.60	0.80	0.40	0.80
9	Pre-exponent for Volume Diffusion	m^2/s	5.00e-5	9.00e-5	2.00e-5	7.00e-5
10	Act. Energy for Volume Diffusion	kJ/mol	200.00	550.00	200.00	550.00
11	Pre-exponent for Boundary Diffusion	m^2/s	5.00e-14	6.00e-14	5.00e-14	6.00e-14
12	Act. Energy for Boundary Diffusion	kJ/mol	200.00	325.0	200.00	325.0
13	Pre-exponent for Surface Diffusion	m^2/s	1.00e-9	2.00e-9	1.00e-9	2.00e-9
14	Act. Energy for Surface Diffusion	kJ/mol	400.00	500.00	400.00	500.00
15	Pre-exponent for Boundary Mobility	m^2/s	5.00e-14	6.00e-14	5.00e-14	6.00e-14
16	Act. Energy for Boundary Mobility	kJ/mol	300.00	500.00	300.00	550.00
17	Particle Size Radius	m	15.0e-6	25.0e-6	5.0e-6	15.0e-6
18	Stage 1 Cut-off Relative Density		0.80	0.89	0.80	0.89
19	Stage 2 Cut-off Relative Density		0.90	0.99	0.90	0.99

With the initial population set, the GA can then use the objective data (experimental data points) to evolve the population towards an optimal region in the search space. The experimental data points used in this

study are listed in Table III. CIPing data was initially used for both the SOMP and SC powders. The population size, mutation rate, and number of generations were also specified in the GA, as indicated in Table IV.

After each generation, a Bayesian Analysis was conducted to determine how well the population was evolving. Part of the Bayesian Analysis involved determining the eigenvalues of the *a posteriori* model covariance and correlation matrices. When the sum of the eigenvalues reached a limit, the GA could be stopped and the evolved population could be used to create densification and error maps. The maps (relative density vs. pressure and temperature) indicated the processing conditions under which the optimized model was most uncertain. More data at these conditions that would be most useful in developing a more accurate model. Consequently, this procedure provides a method for rapid model development with a minimum of experimentation.

RESULTS AND DISCUSSION

RESULTS FOR MO21373 SC

The density and error maps for the *a priori* model distribution for the SC powder are shown in Figure 2. The largest standard error on the relative density map was 0.131 which occurred in the sintering region. The model was then optimized using only the CIPing data of Table III. The expectation of the activation energy of volume diffusion and yield stress were determined as a function of generation and are shown in figures 3 and 4 respectively. The error bars denote 2σ. The fact that the yield stress is converging to a single value but the other variables are not indicates that for this particular set of optimization data, yield stress is the most sensitive parameter. However, such graphs as figures 3 and 4 do not reveal any information regarding parameter correlation. Table V lists the eigenvalues for the 19 parameters derived from the correlation matrix at generation 50. As indicated, in Table V all of the eigenvalues are near one. This fact would imply that there is no apparent correlation between the variables for this particular data set and thus in order to determine which variables are most sensitive or which densification mechanism is active, one can simply look at the convergence ratio of each variable. Here, the convergence ratio is defined as the variable search range divided by the standard deviation of the population. A convergence ratio defined in this manner would have a value of 3.0 for a random distribution and have a larger value for parameters with a high sensitivity. Figure 5 shows the convergence ratio for each variable as a function of generation where the yield stress is the most sensitive parameter. This is not surprising since in most CIPing conditions, densification is accomplished by particle yielding.

Contour graphs of the relative density and standard error for the SC powder optimized with only CIPing data points are exhibited in Figure 6. The maximum uncertainty in Figure 6 has now dropped to 0.109 in the sintering regime. Thus a sintering experiment at 2225 K for one hour was conducted. The sintering and CIPing data were then used in the GA optimization. Table VI lists the eigenvalues resulting from this optimization. Again, there is no clearly dominant eigenvalue. This indicates that there is no apparent correlation between the variables. However, as shown in Figure 7, the value of the volume diffusion activation energy seems to be converging. Figure 8 shows the evolution of the sensitivity ratio for each variable. Figure 8 indicates that the yield stress and volume diffusion activation energy are the most sensitive or influential parameters. This would be expected from sintering data. The addition of sintering data decreased the maximum standard error from 0.109 to 0.108 as shown in figure 9 and changed the region of greatest error on the contour map. With the sintering data, the greatest error was found in the HIPing regime. HIPing experiments should be executed next at 75 MPa and 1200 K to address the largest model uncertainty.

Table III. The initial experimental processing conditions and final densities used as optimization criteria.

Mo SOMP – CIPing data

Objective	Time (s)	Temp. (K)	Press. (MPa)	Final Rel. Dens.
1	0	298	0.1	
	3600	298	34.47	
	7200	298	0.1	0.324
2	0	298	0.1	
	3600	298	68.94	
	7200	298	0.1	0.42
3	0	298	0.1	
	3600	298	137.88	
	7200	298	0.1	0.487
4	0	298	0.1	
	3600	298	206.82	
	7200	298	0.1	0.525
5	0	298	0.1	
	3600	298	275.76	
	7200	298	0.1	0.621
6	0	298	0.1	
	3600	298	344.7	
	7200	298	0.1	0.731

Mo SC - CIPing data

Objective	Time (s)	Temp. (K)	Press. (MPa)	Final Rel. Dens.
1	0	298	0.1	
	3600	298	68.94	
	7200	298	0.1	0.543
2	0	298	0.1	
	3600	298	137.88	
	7200	298	0.1	0.596
3	0	298	0.1	
	3600	298	206.82	
	7200	298	0.1	0.704
4	0	298	0.1	
	3600	298	275.76	
	7200	298	0.1	0.7
5	0	298	0.1	
	3600	298	344.7	
	7200	298	0.1	0.704

Table IV. The GA parameters used in this optimization.

Parameter	Value
Bit length per variable	14
Population size	200
Bitwise mutation rate	1/100

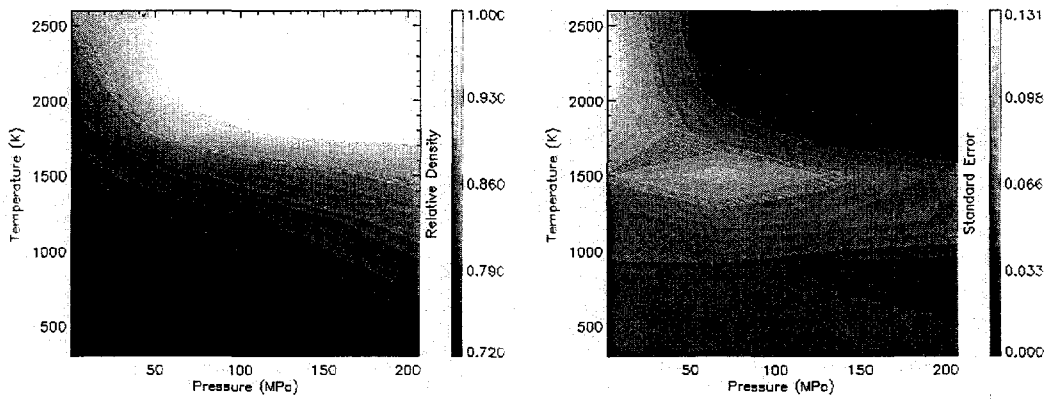

a b

Figure 2a,b. Relative density (a) and standard error (b) contour maps for the *a priori* distribution of the SC powder. The figures were obtained by inserting the model parameter vectors that constituted the *a priori* model distribution into the forward problem for the temperatures and pressures specified assuming one hour ramp up, one hour hold, and one hour ramp down. More experiments are needed in regions with high standard error.

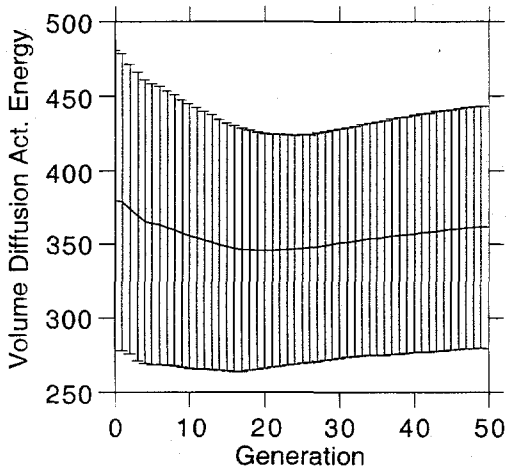

Figure 3. Expectation of activation energy of volume diffusion versus generation for the SC powder optimized using only CIPing data. Error bars represent 2σ. σ remains high, indicating model insensitivity to this parameter.

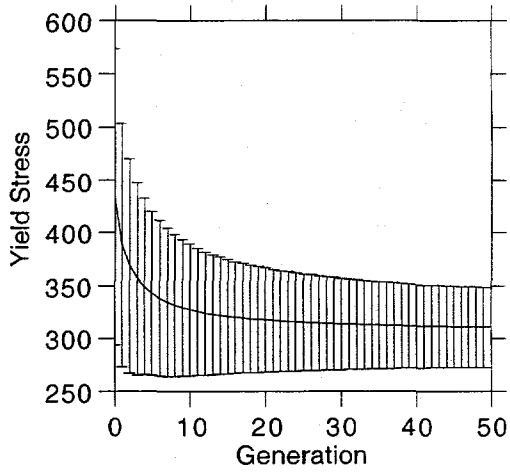

Figure 4. Expectation of yield stress vs. generation number with 2σ for the SC powder optimized using only CIPing data. Population converges quickly to a value, as shown by the decrease in σ.

Table V. The eigenvalues derived from the correlation matrix obtained from the GA optimization with the SC powder using only CIPing data.
The tabular form is for convenience of presentation and not meant to imply a relationship between the rows and columns

0.860209	0.879339	0.893018	0.904266
0.918605	0.932713	0.96610	0.978540
0.985476	1.00026	1.00224	1.00914
1.02058	1.02204	1.06048	1.07523
1.09453	1.11027	1.21443	

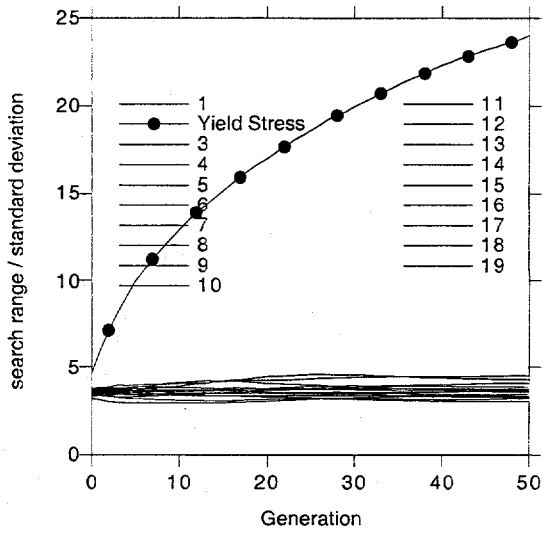

Figure 5. The convergence ratio of each variable for the Mo SC powder model optimized with only CIPing data.

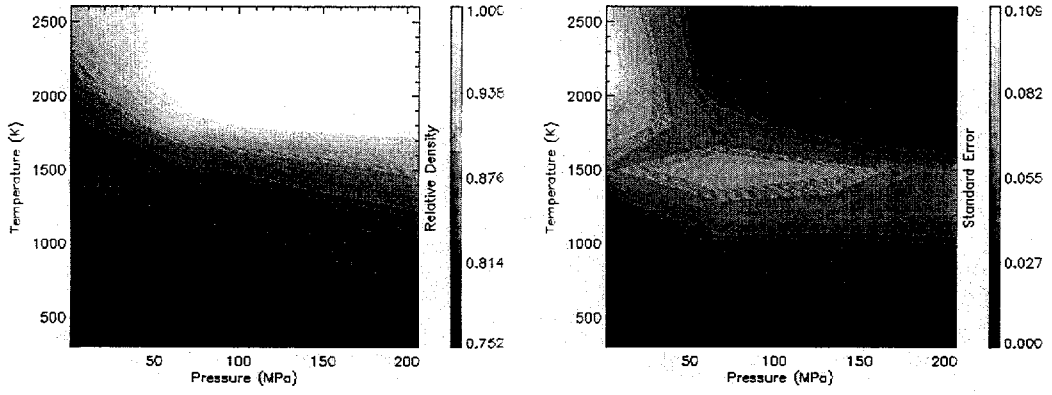

a b

Figure 6a,b. Contour graphs of the expected relative density (a) and associated standard error(b) for a model system evolved using SC powder CIPing data as the objective data points.

Table V. The eigenvalues derived from the correlation matrix obtained from the GA optimization of the SC powder using CIPing and sintering data. The tabular form is for convenience of presentation and not meant to imply a relationship between the rows and columns

0.827451	0.862530	0.869453	0.885045	0.894858	0.918598	0.940347	0.956228
0.960296	0.968496	0.991068	1.00324	1.02953	1.03895	1.06367	1.10954
1.13362	1.17347	1.25542					

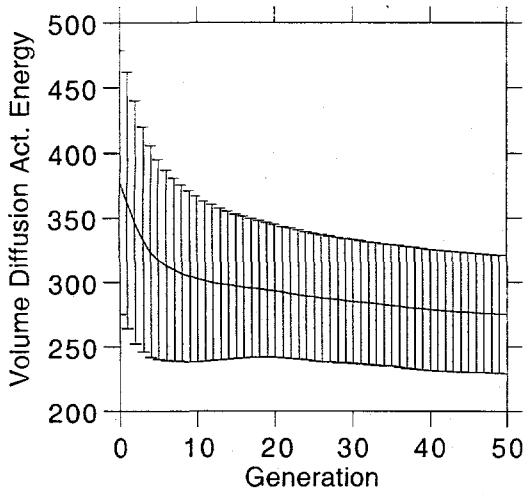

Figure 7. Expectation of the activation energy of volume diffusion with the standard error optimized using both CIPing and sintering data for SC powder.

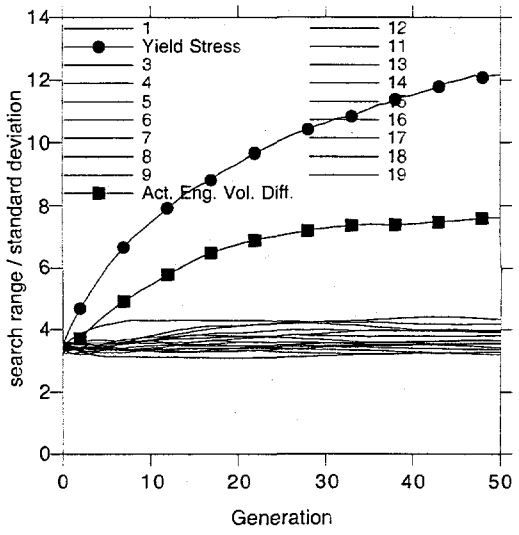

Figure 8. The convergence ratio of each variable for the Mo SC powder model optimized with CIPing and sintering data.

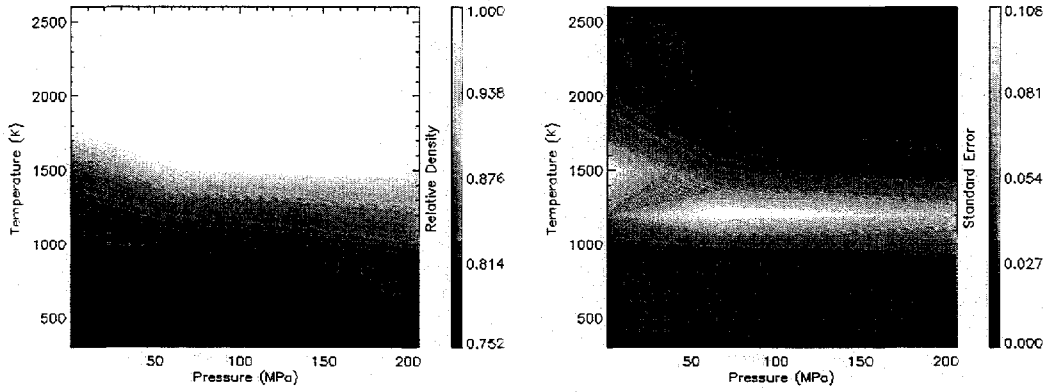

a b

Figure 9a,b. Contour graphs of the expected relative density (a) and associated standard error(b) for a model system evolved using both CIPing and sintering data for SC powder. The standard error graph indicates a need for more experimentation under HIPing conditions.

Results for Mo528 SOMP

Contour maps of the relative density and the associated standard error for the *a priori* distribution of the SOMP powder are shown in Figure 10. The relative density contour graph was obtained by inserting the model parameter vectors that constituted the *a priori* model distribution into the forward problem for the temperatures and pressures specified assuming a one hour ramp up, one hour hold, and one hour ramp down.

Like the SC powder, many of the parameters did not converge to one value, which indicated the insensitivity of the model to these parameters with the data utilized. Graphs of the expectation of activation energy of volume diffusion and yield stress are shown in Figures 11 and 12, respectively. From Figures 11 and 12 and similar graphs for the rest of the variables, the most influential parameter for the model was the yield stress. The activation energy of volume diffusion did not have a large effect upon the model, as was expected with the sole use of CIPing data points.

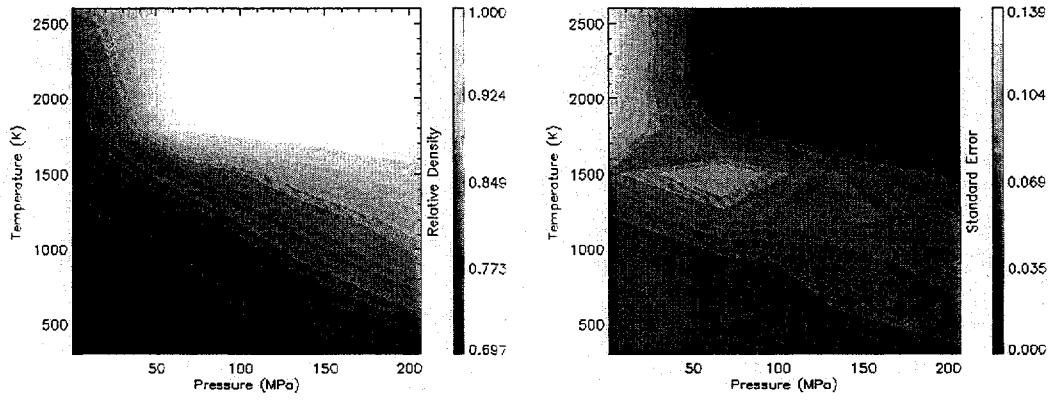

a b

Figure 10a,b. Relative density (a) and standard error (b) contour maps for the *a priori* distribution of the SOMP powder. The figures were obtained by inserting the model parameter vectors that constituted the *a priori* model distribution into the forward problem for the temperatures and pressures specified assuming one hour ramp up, one hour hold, and one hour ramp down. More experiments are needed in regions with high standard error.

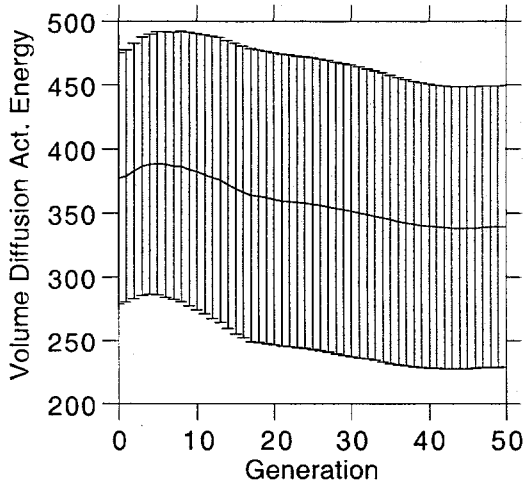

Figure 11. Expectation of activation energy of volume diffusion versus generation for the SOMP powder optimized using only CIPing data. Error bars represent 2σ. The standard deviation remains high, indicating model insensitivity to this parameter.

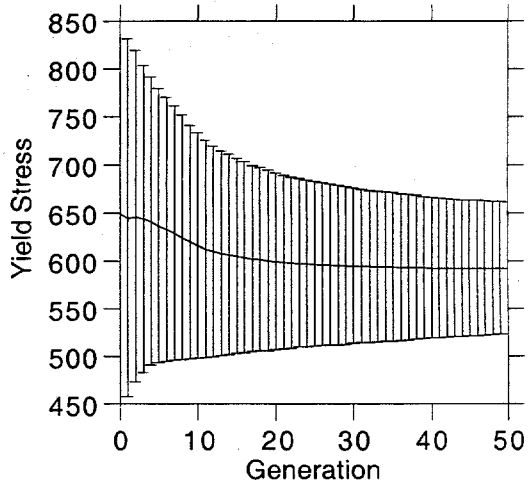

Figure 12. Expectation of yield stress vs. generation number with standard error (2σ) for the SOMP powder optimized using only CIPing data. Population converges quickly to a value, as shown by the decrease in standard error.

As was the case with the SC powder, PCA indicated no significant correlations in the model given the CIPing data set. Likewise, the sensitivity analysis again indicated the most sensitive parameter to be the yield stress.

Densification and error maps for the Mo SOMP powder with CIPing data are shown in Figure 13. The greatest standard error increased from 0.139 in the *a priori* distribution to 0.154 with the CIPing data. The largest uncertainty is found at high temperatures, over 2000 K, and low pressures. Experimental data at these conditions would produce the greatest reduction in error in the model. Accordingly, a sintering experiment, at 2225 K for one hour, was performed, and the results were added to the objectives of the

GA. A similar analysis was performed on the results of the optimization that utilized both CIPing and sintering data as was done with only CIPing data.

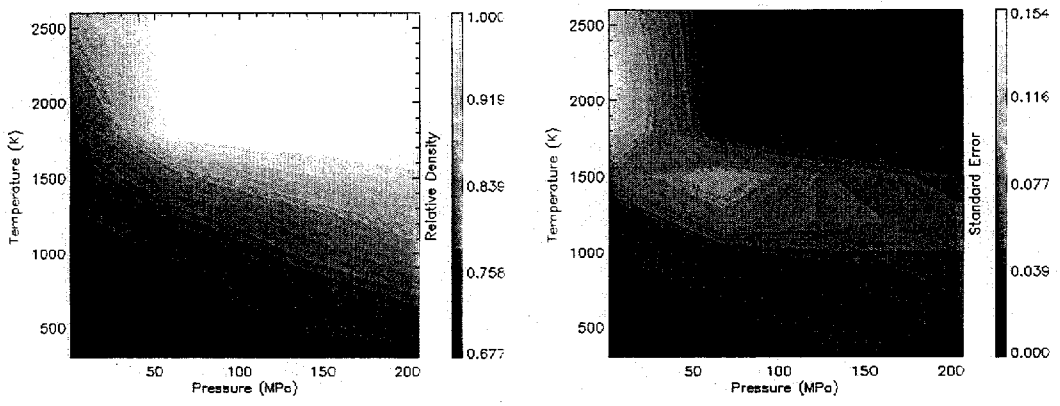

a b

Figure 13a,b. Contour graphs of the expected relative density (a) and associated standard error(b) for a model system evolved using SOMP powder CIPing data as the objective data points.

The yield stress was optimized to the same value with both sets of data. However, as was the case of the SC powder, the activation energy of volume diffusion converged with the addition of sintering data. The contour graphs of relative density and standard error from integrating sintering data into the objectives are exhibited in Figure 14. The standard error was reduced from 0.154 with only CIPing data to 0.047 with the incorporation of the sintering data, and the maximum error moved to the HIPing regime. HIPing experiments should be conducted next at around 75 MPa and 1500 K.

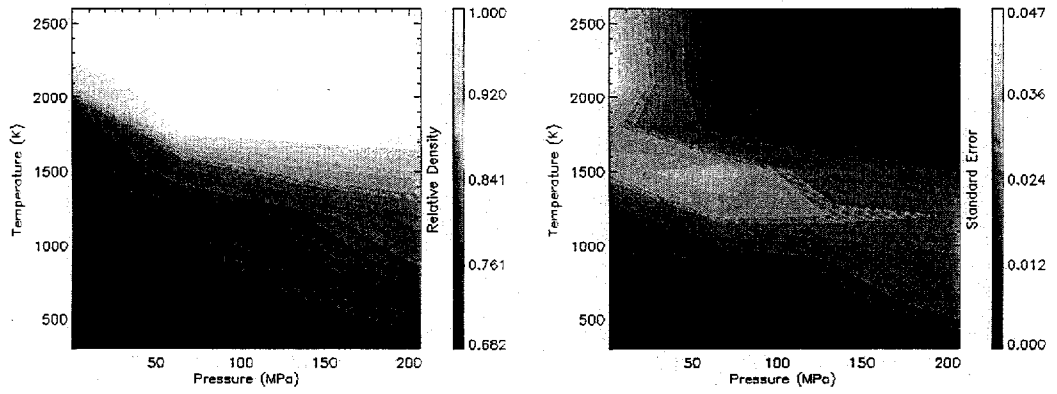

a b

Figure 14a,b. Contour graphs of the expected relative density (a) and associated standard error(b) for a model system evolved using both CIPing and sintering data for SOMP powder. The standard error graph indicates a need for more experimentation under HIPing conditions.

Discussion

As expected, both powders had similar *a priori* densification maps. For both the SC and the SOMP powders, areas at high temperature and high pressure as well as low temperature and low pressure had the same predicted relative density and standard error for all three distributions, namely, the *a priori,* CIPing, and sintering distributions. There are two reasons for this similarity in the contour plots. First, at low temperature and pressures, yielding was the only densification mechanism active, so under these conditions, the model essentially had only one variable to optimize, the yield stress. When the powder models were subjected to sufficiently high temperatures and pressures they densified. Since the relative

density cannot exceed one, there was a large area on the contour graphs with a relative density of one and associated uncertainty of zero.

The individual powder characteristics significantly influenced the optimized model parameters. The average values attained by the GA for yield stress (SC: 310, SOMP:590) were considerably different for the two powders. Mo SC was much closer to the published value of 225.00 MPa than Mo SOMP. With the additional sintering data, activation energy of volume diffusion converged to a similar value for both for powders (275 kJ/mol). Ashby's value for the activation energy of volume diffusion, 405 kJ/mol, was greater than the value attained by the GA with the CIPing and sintering data. This was not wholly a characteristic of the specific powder, but was also an artifact of the model. The model assumed the particles to be fully dense, which was not correct in the case of agglomerates of the SOMP powder. This discrepancy would cause values for activation energies of diffusion to appear smaller than the physical value. Distinct values of parameters were attained for the SC and SOMP powders due to physical differences in the powders, assumptions of the model, and the need for more experimental data. As seen in Figure 1, the particles of the SOMP powder are actually agglomerates, not fully dense particles. This inconsistency might account for part of the discrepancy between the yield stress values for the two powders. Additionally, the effects of impurities in the powders were not included in the model. The higher oxygen content in the SOMP powder should raise the apparent value of the yield stress. Likewise, the presence of a protective oxide layer would act as a barrier to diffusion thus significantly raising the optimal apparent diffusive activation energy of the powder. The reason this did not occur in the optimization was that the agglomerated particles had an unusually high amount of surface energy per unit volume available as a driving force for sintering that was not suggested by the large apparent particle size.

In this work a number of points were brought up that warrant further in depth discussion. One of these points is the fact that the maximum uncertainty of the SOMP study actually went up when CIPing data was used in the optimization. The most likely explanation for this is the fact that the increase in error is simply the result random variation owing to the stochastic nature of the GA procedure itself. It is important to keep in mind that while the maximum error apparently did go up, the uncertainty in the model within the CIPing region of the densification map decreased significantly.

While PCA has been shown to be helpful in determining the degree of correlation of variables, the fact remains that the full utility of PCA in this work has not been exploited or explained in great detail. Optimization of data with a high degree correlation among the variables will display eigenvalues that converge to respective limits with each generation and thus when the sum of the eigenvalues reaches a limit, the optimization can be considered complete. Unfortunately, this work did not have significant correlation in any of the optimizations and thus the convergence criteria could not be adequately shown.

The results of this study show that the GA/BIE technique does an adequate job of handling the inverse and ill-posed problem of optimizing the parameters of the micromechanical HIP model. Furthermore, this work shows that the GA technique is sensitive to minute differences in similar powders and that these differences have the ability to substantially impact the powders' optimal processing conditions. This work also emphasizes the intrinsic limitations of the current model. Namely, a more detailed description of individual powder characteristics such as size distributions and morphologies needs to be incorporated.

CONCLUSIONS

In this study, a Bayesian enhanced GA was used to determine the values of nineteen micromechanical modeling parameters for the sintering of two molybdenum powders. The parameters were then used in the physics of the forward problem to create densification and error maps that indicated the processing regions most in need of more experimental data. Bayesian analysis of the GA output enabled a sensitivity analysis and determination of a GA stopping criteria. This sensitivity analysis is instrumental in identifying not only the active densification mechanisms for each powder but also in understanding how

the morphological differences between the powders contributed to the final discrepancies in relative density even though both Mo samples had the same processing histories.

ACKNOWLEDGEMENTS

Funded by the US Department of Energy and Los Alamos National Laboratory, which is operated by the University of California under contract number W-7405-ENG-36.

REFERENCES

[1] Northcott, L., *Molybdenum*, Academic Press Inc., New York, 1956.

[2] Walters, W.P. and Summers, R.L., "An Analytical Expression for the Velocity Difference Between Jet Particles from a Shaped Charge", *AIP Conference Proceedings*, No.309, Pt.2 (1994), 1861-1864.

[3] Choi, C.S., Prask, H.J., and Orosz, J., Baker, E.L., "Texture Study of two Molybdenum shaped charge liners by neutron diffraction", *Journal of Materials Science*, Vol. 28, 13, 1993, pp. 3557-3563.

[4] Hougstad, B.S. and Dullum, O.S., "Optimization of Shaped Charges", *Journal of Applied Physics,* Vol.55, 1, 1984, pp. 100-106.

[5] Ashby, M. F., "HIP 6.0 Background Reading And Operator Manual," Engineering Department, Cambridge, U. K., 1990.

[6] Reardon, B. J., "Fuzzy Logic versus niched Pareto multiobjective genetic algorithm optimization", *Modelling and Simulation in Materials Science and Engineering,* Vol. 6, 1998, pp. 717-734.

[7] Reardon, B. J., "Optimization of densification modelling paraemters of beryllium powder using a fuzzy logic based multiobjective genetic algorithm", *Modelling and Simulation in Materials Science and Engineering,* Vol. 6, 1998, pp. 735-746.

[8] Reardon, B. J., Bingert, S.R. "Inversion of Tantalum Micromechanical Powder Consolidation and Sintering Models using Bayesian Inference and Genetic Algorithms", *Acta Materialia*, Vol. 48, 2000, pp. 647-658.

[9] Bayes, T., "An essay towards solving a problem in the doctrine of chances", *Phil. Trans. Roy. Soc.* Vol. 53, 1763, pp. 370-418, Vol. 54, 1763, pp. 296-325, reprinted in Biometrika Vol. 45, 1958, pp. 293-315.

[10] Antelman, G., *Elementary Bayesian Statistics,* Eds. A. Madansky, R. McCulloch, and Edward Elgar Publishing, Inc., Lyme, NH, 1997.

[11] Sen, M.K. and Stoffa, P.L., "Rapid Sampling Of Model Space Using Genetic Algorithms : Examples From Seismic Wave-Form Inversion", *Geophysics Journal International*, Vol.108, 1992, pp. 281-292.

[12] Sen, M.K. and Stoffa, P.L., "Bayesian inference, Gibbs' sampler and uncertainty estimation in geophysical inversion", *Geophysical Prospecting*, Vol. 44, 1996, pp. 313-350

[13] Sen, M.K., Bhattacharya, B.B., and Stoffa, P.L., "Nonlinear Inversion Of Resistivity Sounding Data", *Geophysics*, Vol. 58, 4, 1993, pp. 496-507.

[14] Mallick, S., "Model-Based Inversion Of Amplitude-Variations-With-Offset Data Using A Genetic Algorithm", *Geophysics*, Vol. 60, 4, 1995, pp. 939-954.

[15] Gerstoft, P. and Mecklenbraeuker C.F., "Ocean acoustic inversion with estimation of a posteriori probability distributions", *Journal of the Acoustical Society of America*, Vol.104, 2, 1998, pp. 808-819.

[16] Jolliffe, I.T., *Principal Component Analysis,* Springer Series in Statistics, Springer-Verlag New York, Inc. 1986.

[17] Goldberg, D.E., *Genetic Algorithms in Search, Optimization, and Machine Learning*, Addison-Wesley Publishing Company, Inc., New York 1989.